nanomaterials

MDPI

Article

Transparent Platinum Counter Electrode Prepared by Polyol Reduction for Bifacial, Dye-Sensitized Solar Cells

Alvien Ghifari, Dang Xuan Long, Seonhyoung Kim, Brian Ma and Jongin Hong *

Department of Chemistry, Chung-Ang University, 84 Heukseok-ro, Dongjak-gu, Seoul 06974, Korea; alvien.ghifari@gmail.com (A.G.); dxlong.bk@gmail.com (D.X.L.); kimsh9560@gmail.com (S.K.); kehgeeng@gmail.com (B.M.)

* Correspondence: hongj@cau.ac.kr; Tel.: +82-2-820-5869

Received: 7 February 2020; Accepted: 3 March 2020; Published: 11 March 2020

Abstract: Pt catalytic nanoparticles on F-doped SnO_2/glass substrates were prepared by polyol reduction below 200 °C. The polyol reduction resulted in better transparency of the counter electrode and high power-conversion efficiency (PCE) of the resultant dye-sensitized solar cells (DSSCs) compared to conventional thermal reduction. The PCEs of the DSSCs with 5 μm-thick TiO_2 photoanodes were 6.55% and 5.01% under front and back illumination conditions, respectively. The back/front efficiency ratio is very promising for efficient bifacial DSSCs.

Keywords: dye-sensitized solar cell; counter electrode; bifacial; platinum; ethylene glycol

1. Introduction

Dye-sensitized solar cells (DSSCs) have shown promise as low-cost photovoltaics compared to commercially available Si solar cells. They hold great potential for building-attached photovoltaics (BAPVs) and building-integrated photovoltaics (BIPVs), because of their adjustable color/transparency and superior performance in dim light [1–4]. Recently, bifacial DSSCs, which can convert incoming sunlight to electricity through both front and back sides, have been an attractive alternative for photovoltaic devices [5,6]. The standard DSSC consists of a substrate coated with transparent conducting oxides (TCOs), a dye-grafted mesoscopic TiO_2 photoanode, a platinized counter electrode (CE), and an electrolyte containing a redox couple. Among the key components, the CE plays a prominent role in maintaining a flow of current by regenerating the redox mediator. Unfortunately, Pt is a highly expensive and scarce metal, and thus alternative materials, including carbon-based materials [7,8], transition metal compounds [9], conducting polymers [10,11], and their composites [12,13] have been explored.

Nevertheless, Pt is still favored because of its superior electrocatalytic activity and good conductivity. The conventional methods for preparing Pt CEs are vacuum sputtering of a Pt target and thermal decomposition of a platinic acid (H_2PtCl_6) precursor [14,15]. However, these high-energy-consuming approaches increase the cost and energy payback time of DSSCs. In addition to logistical issues, the light absorption at the Pt CEs should be minimized for bifacial operation. Therefore, it is crucial to develop new preparation methods for highly transparent Pt CEs at low temperatures.

Polyol-based synthesis is a versatile and straightforward liquid-phase method that uses high-boiling and multivalent alcohols to synthesize nanomaterials without the requirements of high pressure and autoclaves [16,17]. Polyol can simultaneously act as a reducing agent and water-equivalent solvent. Its chelating ability or controlling the nucleation of nanomaterials. For example, Ouyang and coworkers reported nanostructured Pt CEs prepared by polyol reduction of H_2PtCl_6 in ethylene glycol

(EG) [18,19]. They also utilized EG vapor for solventless chemical reduction of the platinum precursor below 200 °C [20]. Song et al. employed the hydrolysis of urea in a two-step EG solution reduction to achieve uniform dispersion and a smaller size of Pt nanoparticles on conducting glass substrates [21]. Unfortunately, the Pt CEs were prepared by drop-casting the EG-based Pt precursor solution. It has proven challenging to prepare a thin layer of Pt nanoparticles and thus provide highly transparent CEs for the bifacial DSSCs. Therefore, we prepared a highly transparent Pt counter electrode by spin-coating a platinic EG solution and further chemical reduction below 200 °C. We also investigate the photovoltaic performance of the DSSCs from the viewpoint of bifacial operation.

2. Materials and Methods

2.1. Fabrication of Pt Counter Electrodes

F-doped SnO_2 (FTO) glass (TEC 8, Pilkington; sheet resistance = 8Ω/□) substrates were ultrasonically cleaned using acetone, isopropyl alcohol, and deionized water. The substrates were baked at 150 °C for 10 min to completely remove residual water. Then 10 mM platinic acid in ethylene glycol was spin-coated on the FTO substrates. Subsequently, the sample was placed in a muffle furnace and heated to a certain temperature (e.g., 130, 150, 170, 190, and 210 °C). The annealing was maintained for 12 h, and then the sample was cooled down to room temperature. For comparison, 40 mM of the platinic acid solution in 2-propanol was prepared and then spin-coated on the same substrates, followed by heating at 425 °C for 1 h in the muffle furnace [22–24]. The schematic diagram of Pt CE preparation is shown in Figure 1.

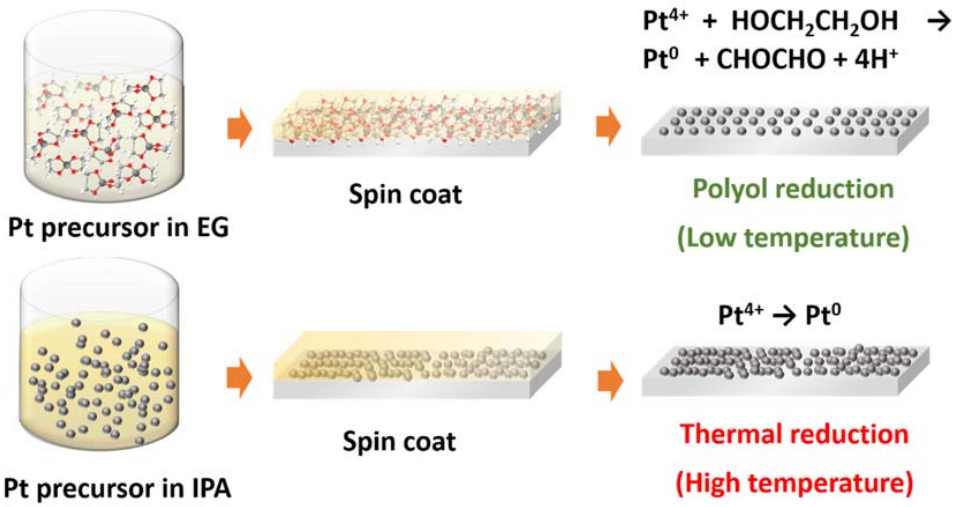

Figure 1. Schematic diagram of counter electrode preparation: polyol reduction (PR) and thermal decomposition (TD).

2.2. Characterization

The surface images of the fabricated Pt CEs were obtained using a field-emission scanning electron microscope (FE-SEM; Sigma, Carl Zeiss AG, Oberkochen, Germany). X-ray photoelectron spectroscopy (XPS) spectra were acquired using a Thermo Scientific K-alpha XPS system (Waltham, MA, United States) with an Al Kα X-ray source monochromator (1486.6 eV). The optical transmittance spectra were recorded using UV/Vis spectroscopy (V-730, JASCO, Tokyo, Japan). An electrochemical measurement station (CompactStat, Ivium Technologies, Eindhoven, The Netherlands) was used to conduct all electrochemical characterization. Cyclic voltammetry (CV) was recorded at a scan rate of 50 mV/s with a three-electrode system that consists of a Pt CE as a working electrode, a Pt wire as a counter electrode, and Ag/AgCl as a reference electrode. A solution of 10.0 mM LiI, 1.0 mM I_2, and 0.1 M $LiClO_4$ in CH_3CN was used as the electrolyte to investigate the electrocatalytic properties of

the Pt CEs for redox reactions. Tafel and electrochemical impedance spectroscopy (EIS) measurements were performed on symmetric cells consisting of CE|electrolyte|CE. Tafel polarization measurements were conducted at a scan rate of 10 mV/s. In EIS measurements, a 10 mV amplitude sinusoidal potential perturbation was input over a frequency range from 1 MHz to 0.1 Hz at zero bias potential. The EIS spectra were analyzed using the equivalent circuit fitting routine in the ZView software (AMETEK, Leicester, UK).

2.3. Device Fabrication and Characterization

The FTO glass substrates were cleaned with O_2 plasma for 10 min, dipped in an aqueous solution of 40 mM $TiCl_4$ at 75 °C for 30 min, and then rinsed several times with deionized water. The TiO_2 paste (Transparent TiO_2, ENBKOREA, Gumi, Korea) was screen-printed on the FTO glass, and the printed film was calcinated at 300 °C for 30 min and 575 °C for 1 h in the muffle furnace. The final areas of the TiO_2 photoanodes were 0.2025 cm^2. The photoanodes were treated in the $TiCl_4$ solution and then heated at 500 °C for 30 min on a hot plate. After O_2 plasma treatment, the photoanodes were dipped into a 0.5 mM dye solution of cis-diisothiocyananoto-bis(2,2-bipyridyl-4,4′-dicarboxylate) ruthenium(II) (N719, Merck KGaA, Darmstadt, Germany) in ethanol for 24 h. The dye-grafted photoanode and Pt CE were assembled with 25 μm-thick thermoplastic film (Surlyn, Solaronix, Aubonne, Switzerland) and sealed by heating. An iodide-based redox electrolyte (Iodolyte AN-50, Aubonne, Switzerland) was injected into the pre-drilled holes in the side of the counter electrode and then sealed. The photovoltaic characteristics were investigated under AM 1.5 global one sun illumination (100 mW/cm^2) using a solar cell I–V measurement system (K3000 LAB, McScience, Suwon, Korea). The photocurrent density (J_{sc}), open-circuit voltage (V_{oc}), fill factor (FF), and power conversion efficiency (η) were recorded simultaneously. Monochromatic incident photon-to-current conversion efficiency (IPCE) was collected to evaluate the spectral response of the solar cells (K3100, McScience, Suwon, Korea). EIS measurement on the fabricated devices was carried out by the same protocol mentioned above.

3. Results

Polyol-based synthesis is a versatile technique to prepare Pt nanostructures. In this study, EG was chosen as the solvent and reducing agent of Pt precursors because of its low boiling point and viscosity. Also, byproducts from the EG reduction, such as glycoaldehyde and diacetyl, could be easily removed [25]. Figure 2a–f shows the surface of the FTO glass substrates decorated with Pt nanoparticles formed by polyol reduction at different temperatures (130, 150, 170, 190, and 210 °C) and thermal decomposition at 425 °C (hereafter, "polyol-reduced" is abbreviated as "PR" and "thermally decomposed" is abbreviated as "TD"). Tiny Pt nanoparticles (<10 nm) were formed and dispersed on the FTO surface for all reaction temperatures. The chemical reduction by EG allows for depositing Pt nanoparticles at low temperatures, and is thus feasible for plastic substrates. As the reduction temperature increased, the aggregation of the Pt nanoparticles diminished, and no aggregation could be observed at the temperature of 190 °C. This indicates that the slower evaporation of EG could result in the growth of larger nanoparticles, more agglomeration, and dendrites. However, the aggregated nanoparticles appeared again at a temperature higher than the boiling point of EG (i.e., 197 °C) because of the inability to control particle nucleation and growth at the elevated temperature [17]. Also, the pyrolysis of H_2PtCl_6 at 425 °C directly led to the formation of large Pt nanoparticles prominently populating the FTO. Accordingly, we predict that their size and distribution will affect the transparency and catalytic activity of the resultant electrodes.

XPS was performed to determine the formation of metallic Pt during our chemical reduction. In Figure 3, the spectra of survey XPS indicates that the samples contained Sn, O, Pt, and Cl—no other elements except carbon were detected. Carbon can result from precursors or sample handling. Interestingly, as the reduction temperature increased, the signal for Cl 2p related to ionic Pt species decreased and then disappeared. Narrow XPS scans of the Pt-4f core level region are also provided in Figure 3. The C 1 s peak at 285.0 eV was used to calibrate all the XPS data. The Pt 4f signal is composed

of three pairs of deconvoluted doublets. The first doublet (71.4 eV and 74.8 eV) corresponds to the platinum in the zero-valent state (i.e., Pt(0)), while the second doublet (72.3 eV and 75.6 eV) can be assigned to platinum in the 2+ valence state (i.e., Pt(II)) [26]. The third (73.7 eV and 77.0 eV) is caused by the Pt^{4+} species, such as $[PtCl_6]^{2-}$, on the surface (i.e., Pt(IV)) [27]. Table 1 summarizes the binding energies and relative integrated peak areas of the deconvoluted peaks at the Pt-4f core level region. The increase in the reduction temperature resulted in the change in the valence state from Pt^{2+} to Pt^0. After the polyol reaction, the Pt species clustered together with different compositions. Accordingly, the reaction temperature is of significant importance in preparing metallic Pt nanoparticles.

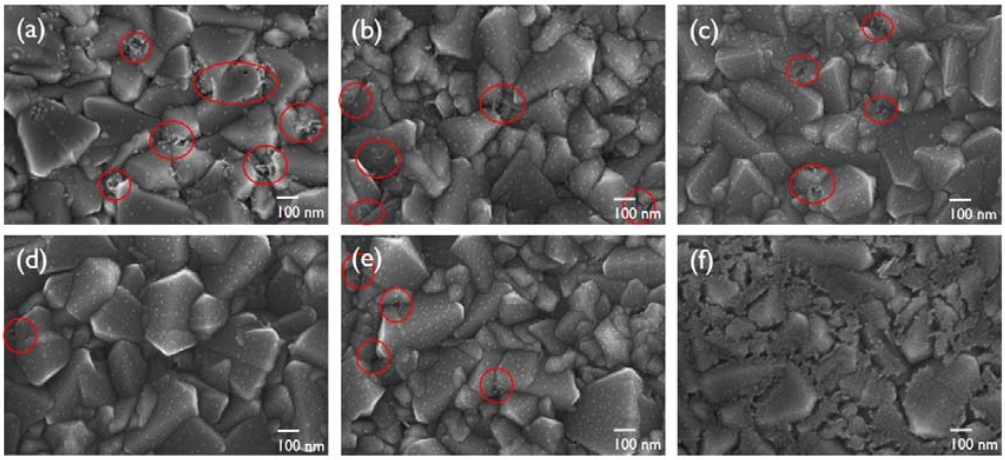

Figure 2. Field-emission scanning electron microscope (FE-SEM) images of Pt films on FTO substrates: (**a**) PR-130, (**b**) PR-150, (**c**) PR-170, (**d**) PR-190, (**e**) PR-210, and (**f**) TD-425.

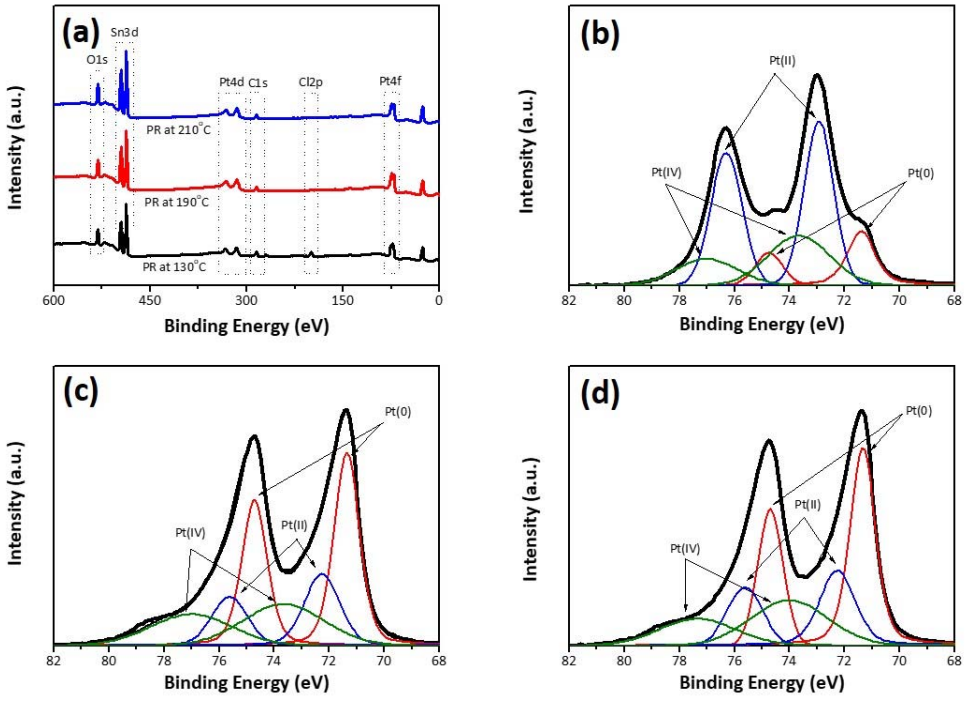

Figure 3. X-ray photoelectron spectroscopy (XPS) scans of polyol-reduced Pt on FTO substrates: (**a**) survey, (**b**) PR-130, (**c**) PR-190, and (**d**) PR-210.

Table 1. Binding energies (eV) and relative proportions (S, in %) of each component measured by XPS.

	Pt(0)			Pt(II)			Pt(IV)		
	$4f_{5/2}$	$4f_{7/2}$	S	$4f_{5/2}$	$4f_{7/2}$	S	$4f_{5/2}$	$4f_{7/2}$	S
PR-130	74.8	71.4	23.7	76.3	72.9	38.8	77.0	73.7	37.5
PR-190	74.7	71.4	48.4	75.6	72.3	22.7	77.0	73.7	28.9
PR-210	74.7	71.4	44.8	75.6	72.3	20.9	77.0	73.7	34.3

In the DSSC operation, an I_3^-/I^- redox couple is commonly utilized as a redox mediator. The CE should collect electrons from the external circuit and effectively catalyze the reduction of I_3^- to I^-. The electrocatalytic activity of the PR CEs was determined using cyclic voltammetry (CV), as shown in Figure 4a. All CV curves show two typical pairs of oxidation and reduction peaks (Ox-1/Re-1 and Ox-2/Re-2), which are described by Equations (1) and (2), respectively [28]:

$$I_3^- + 2e^- \rightleftharpoons 3I^- \quad (1)$$

$$3I_2 + 2e^- \rightleftharpoons 2I_3^- \quad (2)$$

The catalytic reduction activity of the CE can be determined by the first oxidation and reduction peaks (Ox-1 and Re-1). Its electrochemical reversibility can be assessed from the peak-to-peak separation (ΔE_p), which is the difference between the anodic and cathodic peak potentials. A smaller ΔE_p reflects the higher electrocatalytic activity of the CE.

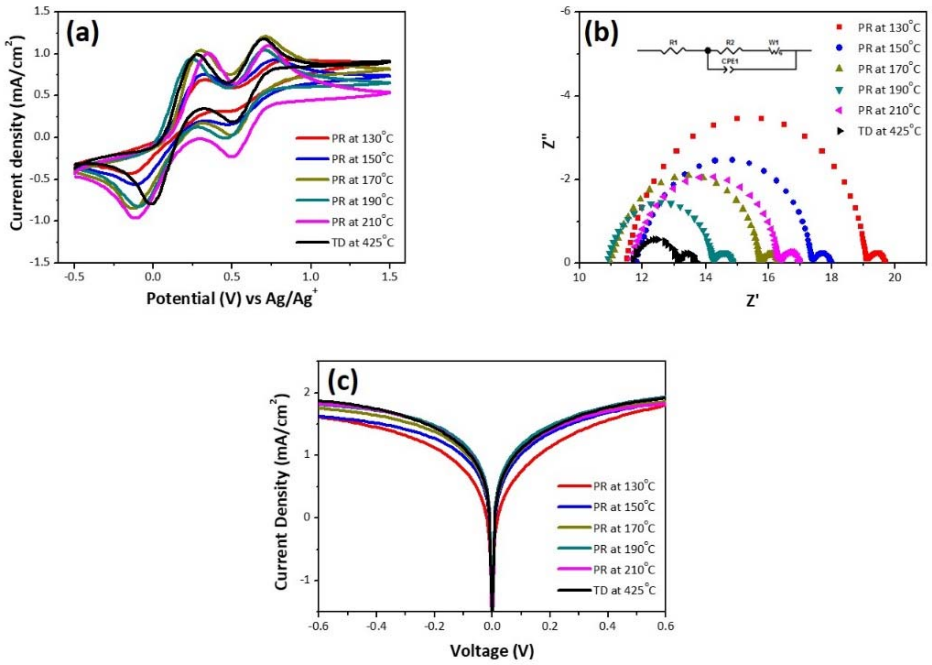

Figure 4. (**a**) Cyclic voltammograms for the redox of I_3^-/I^- species, (**b**) electrochemical impedance spectroscopy (EIS) Nyquist plots for the symmetric cells, and (**c**) Tafel polarization curves.

EIS measurements were also conducted using the symmetrical cells constructed with two identical electrodes. The Nyquist plots (Figure 4b) consist of two apparent semicircles at a high frequency (first semicircle) and a low frequency (second semicircle), respectively. The Randles-type circuit (insert in Figure 4b) was used to simulate the plots. The corresponding parameters are summarized in Table 2. R_s is the series resistance, and can be derived by the intercept of the high-frequency semicircle on the real axis (Z' axis). R_{ct} is the charge transfer resistance at the interface between CE and electrolyte, and can be determined from the radius of the first semicircle on the real axis. All the PR-CEs have nearly

the same R_s, and thus its effect on photovoltaic performance can be ignored. A smaller R_{ct} accelerates triiodide reduction, and thus the PR-190 CE has the superior catalytic activity. The low-frequency semicircle results from Nernst diffusion impedance (Z_N) of the redox species in the electrolyte, which is inversely proportional to the diffusion coefficient of I_3^- in the cells [28]. The decrease in Z_N leads to an increase in the electrocatalytic activity of the CE.

Table 2. Electrochemical parameters of polyol-reduction Pt films at different reaction temperatures.

No	ΔE_p (V)	J_0 (mA/cm^2)	J_{lim} (mA/cm^2)	R_s (Ω/cm^2)	R_{ct} (Ω/cm^2)	Z_N (Ω/cm^2)
PR-130	0.47	4.99	0.21	8.05	5.19	0.44
PR-150	0.44	9.16	0.21	8.26	3.79	0.44
PR-170	0.43	11.14	0.24	7.69	3.21	0.41
PR-190	0.35	14.76	0.26	7.63	2.23	0.44
PR-210	0.46	12.44	0.26	8.13	3.17	0.48
TD-425	0.29	11.62	0.27	11.79	1.27	0.59

Figure 4c shows Tafel polarization plots of the symmetrical cells comprising the Pt CEs and I_3^-/I^- electrolytes. The Tafel plot can be separated into three consecutive zones: polarization, Tafel, and limit diffusion zones. The Tafel and limit diffusion zones are valuable for obtaining both the limiting current density (J_{lim}) and current density (J_0), which correlate with the electrocatalytic activity of the CEs [29]. The intersection of the cathodic branch and the equilibrium potential line can be considered J_0, and thus the steep Tafel slope implies a large J_0. Theoretically, J_0 can also be calculated using Equation (3):

$$J_0 = \frac{RT}{nFR_{ct}} \tag{3}$$

where R is the gas constant, T is the absolute temperature, n is the number of electrons participating in the electrochemical reduction of I_3^-, and F is Faraday's constant. In the limit diffusion zone, J_{lim} can be determined by the intersection of the cathodic branch and the y-axis. J_{lim} is directly proportional to a diffusion coefficient of I_3^- (D) at the same potential, and can be expressed as Equation (4):

$$J_{lim} = \frac{2neDCN_A}{l} \tag{4}$$

where e is the elementary charge, C is the concentration of I_3^-, N_A is the Avogadro constant, and l is the distance between two electrodes. Notably, the values of J_0 and J_{lim} followed the same trend observed in both CV and EIS analyses. Accordingly, the electrocatalytic activity of I_3^-/I^- is as follows: PR-190 > PR-170 > PR-210 > PR-150 > PR-130.

The light absorption at the counter electrode should be minimized to improve light harvesting in the bifacial DSSCs. Figure 5a shows the transmittance spectra of the prepared Pt CEs and bare FTO glass. Polyol reduction manifested higher transparency compared to thermal decomposition in the whole visible light regime, which will be beneficial to bifacial applications. Unfortunately, the increase in reduction temperature resulted in the decrease in transmittance of PR CEs. We think that metallic Pt nanoparticles possibly have a negative effect on the light transparency. Figure 5b,c shows, respectively, the current density-voltage (J–V) characteristics and IPCE spectra of the DSSCs (5 µm-thick TiO_2), which were illuminated from the TiO_2 photoanode side (i.e., front illumination). The photovoltaic parameters of the front- and rear-illuminated DSSCs are summarized in Table 3. The improved electrocatalytic activity of the PR–Pt CE resulted in better photovoltaic performance: power conversion efficiency (η) increased from 5.50% (PR-130) to 6.55% (PR-190). Also, PR-190 exhibited better photovoltaic performance than TD-425 because of the improvement of R_s and Z_N related to the electrocatalytic activity of the CE. It should be noted that all the DSSCs employing PR–Pt CEs maintained more than 76% of their front-illumination efficiency when lit from the Pt CE side (i.e., back illumination). The decrease of η in the back-illumination condition is related to the transmission losses due to the

Pt-based electrocatalyst and the I_3^-/I^- electrolyte [6]. The ratio of the back-illumination efficiency to the front-illumination efficiency ($\eta(R)$) followed the trend of the transmittance of the PR–Pt CEs observed above.

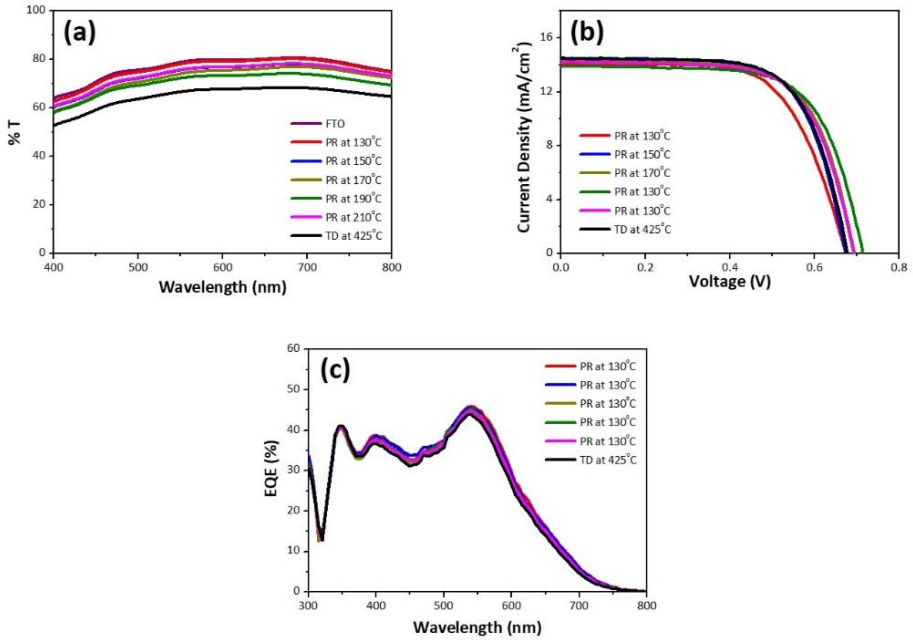

Figure 5. (**a**) Transmittance spectra of the Pt counter electrodes, (**b**) J–V characteristic curves of the dye-sensitized solar cells (DSSCs) (5 µm-thick TiO_2) under one sun front illumination, and (**c**) their incident photon-to-current conversion efficiency (IPCE) spectra.

Table 3. Photovoltaic parameters of DSSCs (5 µm-thick TiO_2) with different Pt counter electrodes [a].

No	Illumination	V_{oc} (V)	J_{sc} (mA/cm^2)	*FF* (%)	η (%)	η (*R*) (%)
PR-130	Front	0.666 ± 0.007	13.82 ± 0.23	59.70 ± 5.48	5.50 ± 0.66	81.03 ± 1.68
	Back	0.664 ± 0.008	10.67 ± 0.32	62.74 ± 4.85	4.45 ± 0.50	
PR-150	Front	0.673 ± 0.003	13.99 ± 0.51	67.45 ± 1.43	6.35 ± 0.33	77.57 ± 1.57
	Back	0.670 ± 0.004	10.65 ± 0.62	69.04 ± 1.22	4.93 ± 0.35	
PR-170	Front	0.694 ± 0.006	13.96 ± 0.31	67.20 ± 1.33	6.51 ± 0.30	76.73 ± 1.33
	Back	0.689 ± 0.003	10.62 ± 0.52	68.28 ± 0.90	5.00 ± 0.30	
PR-190	Front	0.702 ± 0.011	13.77 ± 0.12	67.66 ± 1.55	6.55 ± 0.28	76.61 ± 3.24
	Back	0.699 ± 0.00	10.44 ± 0.23	68.71 ± 1.76	5.01 ± 0.24	
PR-210	Front	0.695 ± 0.004	13.76 ± 0.45	67.02 ± 0.84	6.41 ± 0.29	76.70 ± 2.14
	Back	0.692 ± 0.008	10.42 ± 0.68	68.22 ± 0.94	4.92 ± 0.3	
TD-425	Front	0.682 ± 0.00	13.97 ± 0.46	67.36 ± 0.72	6.42 ± 0.28	67.92 ± 2.66
	Back	0.672 ± 0.005	9.40 ± 0.16	68.97 ± 0.66	4.35 ± 0.05	

[a] The parameters were obtained from at least five cells fabricated with each CE condition; each cell was measured five times.

To date, various transparent CEs have been developed for bifacial applications, such as photovoltaic windows and façades. Table 4 shows the photovoltaic performance of the bifacial DSSCs with platinum and non-platinum CE materials compared to our work. Although DSSC fabrication conditions (e.g., TiO_2 thickness, dyes, electrolytes) are not the same, our polyol reduction technique proved sufficient for fabricating bifacial DSSCs.

Table 4. Photovoltaic parameters of bifacial DSSCs with different CE materials.

Material	Method	T (%)	V_{oc} (V)	J_{sc} (mAcm^{-2})	*FF* (%)	*η (front)* (%)	*η (back)* (%)	*η (R)* (%)	Refs.
PEDOT	Electropolymerization	~90 [a]	0.751	14.60	67	7.40	5.23	70.7	[6]
Carbon	Carbonization	~75	0.721	10.52	60	6.07	5.04	83.0	[7]
Ni_3S_4	Hydrothermal	~70	0.700	13.58	65	6.56	4.86	73.9	[9]
PANI/MoS_2	Composite	~63	0.799	17.93	63	7.99	3.40	42.6	[12]
Pt	Photo-reduction	~95	0.810	13.53	66.6	7.29	5.85	80.3	[30]
Pt	Thermal decomposition	~80 [a]	0.757	15.00	70.7	8.02	4.43	55.2	[30]
Pt	Polyol reduction [b]	~80	0.702	13.77	67.6	6.55	5.01	76.6	-

[a] Transmittance was calculated from absorbance. [b] Our work.

4. Conclusions

In this work, highly transparent Pt CEs were prepared using the polyol reduction technique at low temperatures (<200 °C). Our facile and versatile technique provided better electrocatalytic activity and transparency than conventional thermal decomposition methods, and thus brought significant improvement to the photovoltaic performance of the bifacial DSSCs. In particular, the bifacial DSSC with PR-190 attained 6.55% for front illumination and 5.01% for back illumination, while that with TD had 6.42% for front illumination and 4.35% for back illumination. Because our process does not require an elevated temperature, we are currently exploring the fabrication of flexible bifacial DSSCs that employ polymeric substrates. In addition, further optimization (e.g., $[Co(bpy)_3]^{3+/2+}$ electrolytes) should result in better bifacial DSSC performance.

Author Contributions: Conceptualization, A.G. and D.X.L.; methodology, A.G., S.K., and D.X.L.; formal analysis, A.G., S.K., B.M., and D.X.L.; investigation, A.G., D.X.L., and J.H., data curation, A.G. and D.X.L.; writing—original draft preparation, A.G., B.M., and J.H.; writing—review and editing, B.M. and J.H.; visualization, A.G. and J.H.; supervision, J.H.; project administration, J.H.; funding acquisition, J.H. All authors have read and agreed to the published version of the manuscript.

Funding: This research was supported by a National Research Foundation of Korea (NRF) grant funded by the Ministry of Science and ICT (MSIT) of Korea for the First-Mover Program for Accelerating Disruptive Technology Development (NF-2018M3C1B99088457), and the Energy Technology Development program through the Korea Institute of Energy Technology Evaluation and Planning (KETEP), funded by the Ministry of Trade, Industry and Energy (MOTIE) of Korea (No. 20193010014740 and No. 20193020010440).

Acknowledgments: We acknowledge the Chung-Ang University Research Scholarship in 2019.

Conflicts of Interest: The authors declare no conflict of interest.

References

1. Fakharuddin, A.; Jose, R.; Brown, T.M.; Fabregat-Santiago, F.; Bisquert, J. A perspective on the production of dye-sensitized solar modules. *Energ. Environ. Sci.* **2014**, *7*, 3952–3981. [CrossRef]
2. Wu, W.; Wang, J.; Zheng, Z.; Hu, Y.; Jin, J.; Zhang, Q.; Hua, J. A strategy to design novel structure photochromic sensitizers for dye-sensitized solar cells. *Sci. Rep.* **2015**, *5*, 8592. [CrossRef] [PubMed]
3. Freitag, M.; Teuscher, J.; Saygili, Y.; Zhang, X.; Giordano, F.; Liska, P.; Hua, J.; Zakeeruddin, S.M.; Moser, J.E.; Grätzel, M.; et al. Dye-sensitized solar cells for efficient power generation under ambient lightning. *Nat. Photonics* **2017**, *11*, 372–378. [CrossRef]
4. Yuan, H.; Wang, W.; Xu, D.; Xu, Q.; Xie, J.; Chen, X.; Zhang, T.; Xiong, C.; He, Y.; Zhang, Y.; et al. Outdoor testing and ageing of dye-sensitized solar cells for building integrated photovoltaics. *Solar Energy* **2018**, *165*, 233–239. [CrossRef]
5. Li, P.; Tang, Q. Highly transparent metal selenide counter electrodes for bifacial dye-sensitized solar cells. *J. Power Sources* **2016**, *317*, 43–48. [CrossRef]
6. Kang, J.S.; Kim, J.; Kim, J.-Y.; Lee, M.J.; Kang, J.; Son, Y.J.; Jeong, J.; Park, S.H.; Ko, M.J.; Sung, Y.-E. Highly efficient bifacial dye-sensitized solar cells employing polymeric counter electrodes. *ACS Appl. Mater. Interfaces* **2018**, *10*, 8611–8620. [CrossRef]

7. Bu, C.; Liu, Y.; Yu, Z.; You, S.; Huang, N.; Liang, L.; Zhao, X.-Z. Highly transparent carbon counter electrode prepared via an in situ carbonization method for bifacial dye-sensitized solar cells. *ACS Appl. Mater. Interfaces* **2013**, *5*, 7432–7438. [CrossRef]
8. Zhang, Y.; Zhao, Y.; Duan, J.; Tang, Q. S-doped CQDs tailored transparent counter electrodes for high-efficiency bifacial dye-sensitized solar cells. *Electrochim. Acta.* **2018**, *216*, 588–595. [CrossRef]
9. Hu, Z.; Xia, K.; Zhang, J.; Hu, Z.; Zhu, Y. Highly transparent ultrathin metal sulfide films as efficient counter electrodes for bifacial dye-sensitized solar cells. *Electrochim. Acta* **2015**, *170*, 39–47. [CrossRef]
10. Bu, C.; Tai, Q.; Liu, Y.; Guo, S.; Zhao, X. A transparent and stable polypyrrole counter electrode for dye-sensitized solar cell. *J. Power Sources* **2013**, *221*, 78–83. [CrossRef]
11. Li, H.; Xiao, X.; Han, G.; Hou, H. Honeycomb-like poly(3,4-ethylenedioxythiophene) as an effective and transparent counter electrode in bifacial dye-sensitized solar cells. *J. Power Sources* **2017**, *342*, 709–716. [CrossRef]
12. He, B.; Zhang, X.; Zhang, H.; Li, J.; Meng, Q.; Tang, Q. Transparent molybdenum sulfide decorated polyaniline complex counter electrodes for efficient bifacial dye-sensitized solar cells. *Solar Energy* **2017**, *147*, 470–478. [CrossRef]
13. Ahmed, A.S.A.; Xiang, W.; Hu, X.; Qi, C.; Amiinu, I.S.; Zhao, X. Si_3N_4/MoS_2-PEDOT:PSS composite counter electrode for bifacial dye-sensitized solar cells. *Solar Energy* **2018**, *173*, 1135–1143. [CrossRef]
14. Moraes, R.S.; Saito, E.; Leite, D.M.G.; Massi, M.; da Silva Sobrinho, A.S. Optical, electrical and electrochemical evaluation of sputtered platinum counter electrodes for dye sensitized solar cells. *Appl. Surf. Sci.* **2016**, *364*, 229–234. [CrossRef]
15. Zhou, R.; Guo, W.; Yu, R.; Pan, C. Highly flexible, conductive and catalytic Pt networks as transparent counter electrodes for wearable dye-sensitized solar cells. *J. Mater. Chem. A* **2015**, *3*, 23028–23034. [CrossRef]
16. Dong, H.; Chen, Y.C.; Feldmann, C. Polyol synthesis of nanoparticles: Status and options regarding metals, oxides, chalcogenides, and non-metal elements. *Green Chem.* **2015**, *17*, 4107–4132. [CrossRef]
17. Fievet, F.; Ammar-Merah, S.; Brayner, R.; Chau, F.; Giraud, M.; Mammeri, F.; Peron, J.; Piquemal, J.Y.; Sicard, L.; Viau, G. The polyol process: A unique method for easy access to metal nanoparticles with tailored sizes, shapes and compositions. *Chem. Soc. Rev.* **2018**, *47*, 5187–5233. [CrossRef]
18. Cho, S.J.; Ouyang, J. Attachment of platinum nanoparticles to substrates by coating and polyol reduction of a platinum precursor. *J. Phys. Chem. C* **2011**, *115*, 8519–8526. [CrossRef]
19. Sun, K.; Fan, B.; Ouyang, J. Nanostructured platinum films deposited by polyol reduction of a platinum precursor and their application as counter electrode dye-sensitized solar cells. *J. Phys. Chem. C* **2010**, *114*, 4237–4244. [CrossRef]
20. Cho, S.J.; Neo, C.Y.; Mei, X.G.; Ouyang, J.Y. Platinum nanoparticles deposited on substrates by solventless chemical reduction of a platinum precursor with ethylene glycol vapor and its application as highly effective electrocatalyst in dye-sensitized solar cells. *Electrochim. Acta* **2012**, *85*, 16–24. [CrossRef]
21. Song, M.Y.; Chaudhari, K.N.; Park, J.; Yang, D.-S.; Kim, J.H.; Kim, M.-S.; Lim, K.; Ko, J.; Yu, J.-S. High efficient Pt counter electrode prepared by homogeneous deposition method for dye-sensitized solar cell. *Appl. Energy* **2012**, *100*, 132–137. [CrossRef]
22. Decoppet, J.-D.; Moehl, T.; Babkair, S.S.; Alzubaydi, R.A.; Ansari, A.A.; Habib, S.S.; Zakeeruddin, S.M.; Schmidt, H.-W.; Grätzel, M. Molecular gelation of ionic liquid–sulfolane mixtures, a solid electrolyte for high performance dye-sensitized solar cells. *J. Mater. Chem. A* **2014**, *2*, 15972–15977. [CrossRef]
23. Leonardi, E.; Penna, S.; Brown, T.M.; Di Carlo, A.; Reale, A. Stability of dye-sensitized solar cells under light soaking test. *J. Non-Cryst. Solids* **2010**, *356*, 2049–2052. [CrossRef]
24. Veerender, P.; Saxena, V.; Jha, P.; Koiry, S.P.; Gusain, A.; Samanta, S.; Chauhan, A.K.; Aswal, D.K.; Gupta, S.K. Free-standing polypyrrole films as substrate-free and Pt-free counter electrodes for quasi-solid dye-sensitized solar cells. *Org. Electron.* **2012**, *13*, 3032–3039.
25. Skrabalak, S.E.; Wiley, B.J.; Kim, M.; Formo, E.V.; Xia, Y. On the polyol synthesis of silver nanostructures: Glycolaldehyde as a reducing agent. *Nano Lett.* **2008**, *8*, 2077–2081. [CrossRef] [PubMed]
26. Dablemont, C.; Lang, P.; Mangeney, C.; Piquemal, J.-Y.; Petkov, V.; Herbst, F.; Viau, G. FTIR and XPS study of Pt nanoparticle functionalization and interaction with alumina. *Langmuir* **2008**, *24*, 5832–5841. [CrossRef]
27. Liu, Z.; Lee, J.Y.; Chen, W.; Han, M.; Gan, L.M. Physical and electrochemical characterizations of microwave-assisted polyol preparation of carbon-supported PtRu nanoparticles. *Langmuir* **2004**, *20*, 181–187. [CrossRef]

28. Wan, J.; Fang, G.; Yin, H.; Liu, X.; Liu, D.; Zhao, M.; Ke, W.; Tao, H.; Tang, Z. Pt-Ni alloy nanoparticles as superior counter electrodes for dye-sensitized solar cells: Experimental and theoretical understanding. *Adv. Mater.* **2014**, *26*, 8101–8106. [CrossRef]
29. Chang, P.-J.; Cheng, K.-Y.; Chou, S.-W.; Shyne, J.-J.; Yang, Y.-Y.; Hung, C.-Y.; Lin, C.-Y.; Chen, H.-L.; Chou, H.-L.; Chou, P.-T. Tri-iodide reduction activity of shape- and composition-controlled PtFe nanostructures as counter electrodes in dye-sensitized solar cells. *Chem. Mater.* **2016**, *28*, 2110–2119. [CrossRef]
30. Popoola, I.K.; Gondal, M.A.; AlGhamdi, J.M.; Qahtan, T.F. Photofabrication of highly transparent platinum counter electrodes at ambient temperature for bifacial dye sensitized solar cells. *Sci. Rep.* **2018**, *8*, 12864.